Cell

Skin Stem Cells Orchestrate Directional Migration by Regulating Microtubule-ACF7 Connections through GSK3β

Xiaoyang Wu,[1] Qing-Tao Shen,[2] Daniel S. Oristian,[1] Catherine P. Lu,[1] Qinsi Zheng,[1,3] Hong-Wei Wang,[2] and Elaine Fuchs[1,*]
[1]The Howard Hughes Medical Institute and Laboratory of Mammalian Cell Biology and Development, Rockefeller University, New York, NY 10065, USA
[2]Department of Molecular Biophysics and Biochemistry, Yale University, 333 Cedar Street, New Haven, CT 06520, USA
[3]Tri-institutional Training Program in Chemical Biology, Weill Cornell Medical College, New York, NY 10065, USA
*Correspondence: fuchslb@rockefeller.edu
DOI 10.1016/j.cell.2010.12.033

SUMMARY

Homeostasis and wound healing rely on stem cells (SCs) whose activity and directed migration are often governed by Wnt signaling. In dissecting how this pathway integrates with the necessary downstream cytoskeletal dynamics, we discovered that GSK3β, a kinase inhibited by Wnt signaling, directly phosphorylates ACF7, a > 500 kDa microtubule-actin crosslinking protein abundant in hair follicle stem cells (HF-SCs). We map ACF7's GSK3β sites to the microtubule-binding domain and show that phosphorylation uncouples ACF7 from microtubules. Phosphorylation-refractile ACF7 rescues overall microtubule architecture, but phosphorylation-constitutive mutants do not. Neither mutant rescues polarized movement, revealing that phospho-regulation must be dynamic. This circuitry is physiologically relevant and depends upon polarized GSK3β inhibition at the migrating front of SCs/progeny streaming from HFs during wound repair. Moreover, only ACF7 and not GSKβ-refractile-ACF7 restore polarized microtubule-growth and SC-migration to *ACF7* null skin. Our findings provide insights into how this conserved spectraplakin integrates signaling, cytoskeletal dynamics, and polarized locomotion of somatic SCs.

INTRODUCTION

Directional cell movement is essential for developmental morphogenesis, tumor metastasis, and wound repair. A typical migrating cell adopts front-rear polarity with asymmetrical distribution of signaling molecules and cytoskeletal components. During establishment of polarity, temporal capture and stabilization of microtubules (MTs) occur near filamentous actin (F-actin)-enriched leading edges, which enable reorientation of the MT-organizing center and Golgi complex to ensure biased vesicular transport for directional migration (Etienne-Manneville, 2004; Siegrist and Doe, 2007). Among many regulatory molecules required for cell migration, the ubiquitously-expressed serine and threonine kinase glycogen synthase kinase 3β (GSK3β) is particularly important in transmitting upstream signaling necessary for establishing cell polarity and guiding directional movement (Sun et al., 2009).

In contrast to most other protein kinases, GSK3β activity is high in nonstimulated cells, but it is dampened at the leading edge of scratch-wounded astrocytes and endodermal cells in vitro and in developing neurons of brain slices ex vivo (Etienne-Manneville and Hall, 2003; Kodama et al., 2003; Yoshimura et al., 2006). In vitro, GSK3β inhibition and cell polarity are known to be provoked by CDC42 (Etienne-Manneville and Hall, 2003). In vivo, GSK3β activity is inhibited by Wnt signaling, which in turn leads to β-catenin stabilization, which plays a critical and near universal role in stem cell (SC) activation and migration (Fuchs, 2009; Nusse et al., 2008). Despite this tantalizing connection, the possible physiological relevance among Wnt signaling, SC activation, and cytoskeletal remodeling remains unclear. Another key unaddressed question is how GSK3β regulates the dynamic changes in MT organization and stabilization that transpire during polarized movements of somatic SCs.

Hair follicles (HFs) provide an ideal paradigm to address these issues. Adult HFs undergo homeostasis through cyclical bouts of active growth (anagen), regression (catagen), and rest (telogen) (Figure S1A available online). They also participate in epidermal re-epithelialization during wound healing (Blanpain and Fuchs, 2009; Ito et al., 2005; Tumbar et al., 2004). Both processes rely upon a resident population of SCs, which reside in a specific niche called the bulge, located at the base of the noncycling portion of the HF (Figure S1A). Wnt signaling emanating from polarized epithelial-mesenchymal crosstalk in the SC niche is critical for hair follicle stem cell (HF-SC) activation during tissue homeostasis (Greco et al., 2009). In addition, localized Wnt signaling/β-catenin at a wound site initiates the migration of SCs after injury (Ito et al., 2005, 2007). Based upon these points, the potential exists for using skin as a model to dissect how signaling cues to SCs might regulate the cytoskeleton to orchestrate cell polarization and directional cell movement. In searching for potential cytoskeletal regulators in this process, we noticed that HF-SCs display significantly more actin crosslinking

factor-7 (ACF7; also called MACF1, MT and actin crosslinking factor-1) than other skin epithelial cells (Blanpain et al., 2004; Morris et al., 2004; Tumbar et al., 2004) (Figure S1B).

Unique to multicellular organisms, spectraplakins such as ACF7 can bind both MT and actin networks (Jefferson et al., 2004; Röper et al., 2002). Although broadly expressed, their essential functions are most clearly revealed in muscle, neurons and skin epithelial cells, which maintain elaborate yet dynamic cytoskeletal networks. Mutations in the single *Drosophila* spectraplakin gene (Kakapo/short-stop/shot) cause a wide variety of cellular and tissue defects that include perturbations in actin-MT organization, cell-cell adhesion and integrin-mediated epidermal attachment to muscle. There are two evolutionarily conserved mammalian counterparts. Mice lacking BPAG1/dystonin display sensory neuron and muscle degeneration and have gross defects in cytoskeletal organization and function. By contrast, mice lacking ACF7 exhibit early embryonic lethality (Chen et al., 2006; Kodama et al., 2003). Recent studies show that mice conditionally lacking ACF7 display defects in cell migration. This was true for both K14-Cre cKO animals, impaired in skin wound healing (Wu et al., 2008) and for Nestin-Cre cKO mice, defective in brain development (Goryunov et al., 2010).

While the loss of function data underscore the importance of spectraplakins in coordinating the cytoskeletal dynamics necessary for cells to polarize and move in a directed fashion (Rodriguez et al., 2003), the mechanisms underlying the regulation of spectraplakin-mediated actin-MT connections remain unknown. Similarly, lacking are the molecular details of the circuitry that must link upstream signaling pathways to cytoskeletal remodeling in order for SCs to migrate from their niche. In the present report, we make major inroads into understanding this process. We identify a link between GSK3β and ACF7 and further reveal the in vivo relevance of this connection in polarized locomotion of skin stem cells upon injury.

RESULTS

C-Terminal Tail Interactions Govern Binding between ACF7 and Microtubules

ACF7's carboxy-terminal tail (CT) contains a Gas2-related (GAR) domain and a (GSR-repeat domain (GSR) domain. Previous studies suggest, and we have confirmed, that both domains are involved in the interaction with MTs (Sun et al., 2001; Wu et al., 2008). To obtain structural information on this interaction, we incubated ACF7(CT) with polymerized MTs and conducted ultrastructural analyses. Under saturating conditions [4:1 molar ACF7 (CT):tubulin heterodimer], ACF7(CT) markedly enhanced the electron density along the MT surface (Figure 1A). When compared with naked MTs, ACF7(CT)-coated MTs were ~10 nm thicker in diameter (projection profile in Figure 1A). Fourier transform analyses further indicated that whether decorated with ACF7(CT) or not, assembled MTs displayed a 40Å layer line corresponding to the packing of tubulin dimers. However, only ACF7(CT)-decorated MTs displayed discrete 80Å layer lines, suggesting that ACF7 might associate with the MT lattice with a rather weak distinction between α- and β- tubulins (Figure 1A).

Interaction with the MT lattice usually involves the acidic C-terminal tails of tubulin subunits that protrude from the MT surface. To test this hypothesis, we performed binding assays between ACF7(CT) and increasing concentrations of taxol-stabilized MTs. Just prior to adding ACF7(CT), we exposed half the polymerized MTs to subtilisin to shave protruding tubulin tails (MTΔC-tail). Following ultracentrifugation, pellets were then analyzed by SDS-polyacrylamide gel electrophoresis (PAGE) and Coomassie Blue (CB) staining. Subtilisin-treated MTs still pelleted after ultracentrifugation, confirming that MTs remained assembled after treatment. Only a slight increase was noted in tubulin's electrophoretic mobility, consistent with tail removal (compare asterisked lanes in Figure 1B). However, this modification markedly diminished ACF7(CT)'s binding to MTs (Figure 1B). When ACF7(CT)'s concentration was progressively increased, its association with MTs became saturating, reflected by an increase in the soluble pool of free ACF7(CT). A Scatchard plot of the data are shown in Figure 1C. ACF7(CT) binding to untreated MTs gave a K_D of $\sim 1.4 \times 10^{-7}$ M, which was comparable to published results on GAR and GSR domains of ACF7 (Sun et al., 2001). By contrast, the affinity of ACF7(CT) for subtilisin-treated MTs was >10× weaker ($K_D \sim 1.5 \times 10^{-6}$ M).

Phosphorylation of ACF7's C-Terminal Domain by GSK3β

Association with tubulin tails usually depends on electrostatic interactions between acidic tubulin C termini and positively charged surfaces of MT-binding proteins. Consistent with this notion, ACF7(CT) contains many lysine (K) and arginine (R) residues. Particularly, the GSR domain (202 amino acids) harbors 36 strongly basic residues, with a calculated isoelectric point at 11.8. Additionally, 32% of residues in ACF7's GSR domain are serine or threonine, suggestive of the potential to regulate ACF7-MT's electrostatic interactions through protein phosphorylation. To address this possibility, we transfected primary keratinocytes with ACF7(CT) and labeled them with [^{32}P]-orthophosphate. Our results showed that ACF7(CT) is efficiently phosphorylated in vivo (Figure 1D).

We next analyzed phospho-ACF7(CT) by mass spectrometry. We circumvented the difficulties posed by ACF7(CT)'s high percentage of basic residues by choosing protease AspN, which cleaves peptide bonds N-terminal to aspartate. Liquid chromatography-tandem mass spectrometry (LC-MS/MS) identified multiple (up to six) phosphorylation sites within a peptide encompassing the GSR repeats (Figures 1E and 1F). Interestingly, the characteristic GSR repeats within this sequence have six serines that match consensus GSK3β phosphorylation sites [phosphorylation cluster-1 (P1)]. While in silico analysis with different phosphorylation prediction algorithms (Obenauer et al., 2003; Schiller, 2007) revealed additional potential GSK3β sites [phosphorylation cluster 2 (P2), Figure 1F], their incompatible sequence context precluded efficient peptide retrieval for MS/MS analysis.

To determine whether ACF7 is specifically phosphorylated by GSK3, we first tested for an endogenous association between ACF7 and GSK3β proteins in HF-SCs. Immunoblot analyses revealed GSK3β in anti-ACF7 immunoprecipitates of wild-type (WT) but not *ACF7* null cell lysates (Figure 2A). In vitro kinase (IVK) assays further showed that ACF7 is a substrate for active GSK3β and that GSK3β phosphorylates ACF7(CT) but not ACF7-NT (N-terminal domain of ACF7 serving as a control)

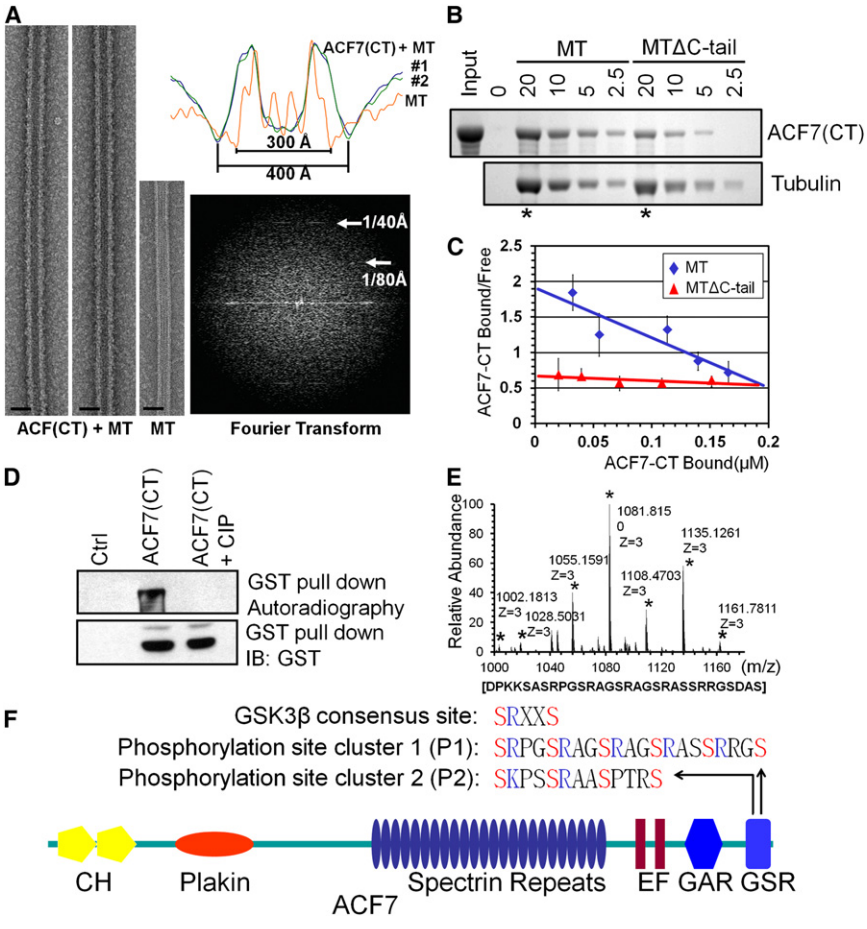

Figure 1. Structural Evidence that Electrostatic Interactions and Phosphorylation May Regulate Associations between ACF7 and MT

(A) Ultrastructural analyses of negatively stained MTs either decorated with ACF7(CT) or naked. Data were normalized and are shown superimposed in the upper right as 1D projection profiles along the MT axis. The scale bars represent 20 nm. A fourier transform of an ACF7-decorated MT is shown with the 40 Å and 80 Å layer lines denoted by white arrows.

(B) Cosedimentation assay with ACF7(CT) and with decreasing amounts (20, 10, 5, and 2.5 μg) of MTs ± subtilisin. Note small downshift of tubulin bands (asterisks) and also decreased binding to ACF7(CT) that occurs following enzymatic treatment of polymerized MTs. MTΔC-tail indicates MT with C-terminal tail removed by subtilisin.

(C) Dissociation constants (Kd) of ACF7's interactions with MT ± subtilisin. Binding assays were performed as in (B) but with a range of ACF7(CT) concentrations. Scatchard plot represents average of three data sets.

(D) GST-tagged ACF7(CT) was purified from [^{32}P] orthophosphate-labeled keratinocyte lysates ± calf intestine alkaline phosphatase (CIP) and subjected to autoradiography and immunoblotting (IB).

(E) Tandem mass spectrometry peptide mass map of AspN-generated peptides from purified ACF7 (CT) protein. Stars (★) denote multiple signals corresponding to a serine-rich phospho-peptide, whose deduced sequence is shown.

(F) Diagram of ACF7 with its many domains. The following abbreviations are used: CH, calponin homology F-actin binding; EF: EF hand motif mediating potential Ca^{2+} binding; GAR-GSR, Gas2-related and GSR repeats for MT binding. GSR repeats contain two potential GSK3β phosphorylation clusters, shown here, aligned with consensus GSK3β site (phospho-Ser in red, requisite Arg in blue). Figure 1 is associated with Figure S1.

(Figure 2B). Moreover, coexpression of GSK3β with ACF7(CT) in cultured cells resulted in phosphorylation of ACF7 that was sensitive to treatment of phosphatase (Figure 2C).

To assess whether our identification of GSK3β phosphorylation sites in ACF7(CT) was correct, we replaced the predicted GSK3β-targeted serines with alanines and repeated our phosphorylation assays in vitro and in vivo. Individually, mutations in P1 and P2 each reduced overall phosphorylation. Combinatorial mutations of both clusters abolished ACF7(CT) GSK3β phosphorylation (Figures 2D and 2E).

Phosphorylation of ACF7 by GSK3β Inhibits Microtubule Binding

Our finding of functional GSK3β phosphorylation sites in ACF7's GSR domain hinted a potential role of this signaling event in tempering ACF7's MT connection by reducing their electrostatic affinity. To test this possibility, we had to first overcome the technical hurdles of ACF7's enormous size (5380 amino acid residues) and engineer mammalian expression vectors encoding human influenza hemagglutinin epitope (HA)-tagged full-length ACF7 as well as point mutants that converted GSK3β phosphorylation sites at P1 and P2 to either a kinase-refractile version harboring Ser→Ala mutations (S:A mutant) or a phosphomimetic version, containing Ser→Asp mutations (S:D mutant).

We purified the proteins by affinity chromatography (Wu et al., 2008) and carried out in vitro cosedimentation assays with polymerized MTs (Figure 3A). Both HA-tagged ACF7 and its S:A mutant counterpart maintained a strong affinity for MT binding similar to WT ACF7, while ACF7(S:D) exhibited significantly reduced affinity for MTs. Similar results were obtained when the binding assays were repeated with freshly prepared lysates from cells expressing ACF7 or its mutants (Figure 3B). In contrast to the effects of S:A and S:D mutations on MT-binding affinity, ACF7's F-actin-binding affinity and adenosine triphosphate (ATP) hydrolysis activity were unaffected (Figures S2A and S2B).

To directly assess the effects of GSK3β phosphorylation, we next coexpressed constitutively active GSK3β (caGSK3β, S9A mutant) with either WT or kinase-refractile ACF7. As predicted, the MT-binding affinity of WT-ACF7 was reduced when GSK3β was superactivated (Figure 3C). This effect was specific for ACF7's C-terminal GSR domain, since GSK3β did not alter interactions between ACF7(S:A) and MTs (Figure 3C). Consistent with these results, inhibition of endogenous GSK3β activity by

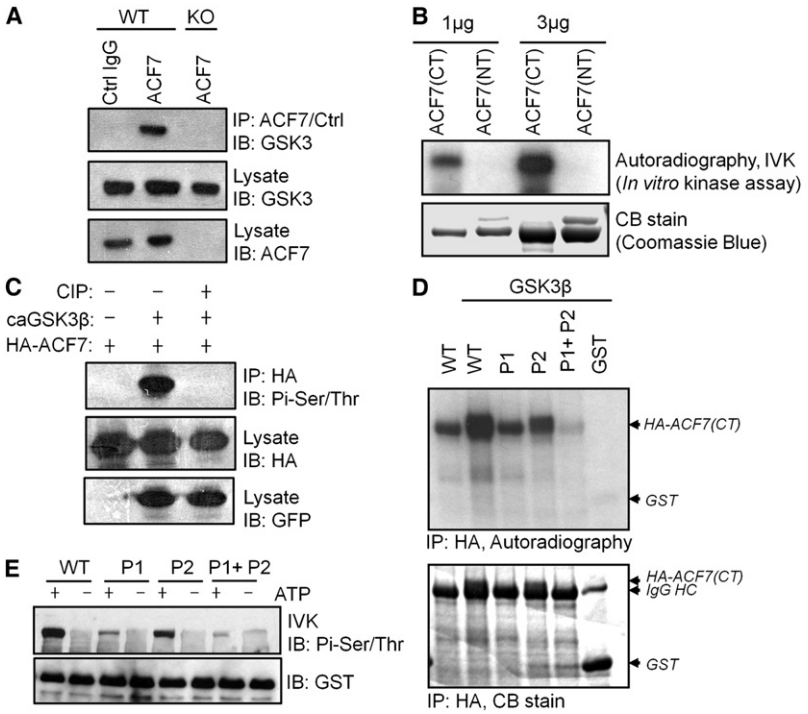

Figure 2. GSK3β Associates with and Phosphorylates ACF7

(A) Bulge SC lysates were analyzed by SDS-PAGE and IB before and after immunoprecipitation (IP) with ACF7 and control IgG Abs. Blots were probed with GSK3β or ACF7 Abs as indicated.

(B) In vitro GSK3β kinase (IVK) assays were performed on C- or N-terminal ACF7. Phosphorylation was analyzed by SDS-PAGE and autoradiography.

(C) Lysates are from cultured cells expressing HA-tagged ACF7(CT) ± constitutively active (ca) GFP-tagged GSK3β (or Ctrl vector) ± CIP phosphatase. Lysates were analyzed ± anti-HA IP by SDS-PAGE and anti-phosphoserine/threonine (Pi-Ser/Thr) immunoblotting.

(D) Cells were transfected with plasmids encoding WT or GSK3-site mutants (see Figure 1F) of HA-tagged ACF7 (CT) (or HA-tagged GST control) and caGSK3β or control vector. After labeling with [^{32}P]-orthophosphate, proteins were subjected to anti-HA IP, SDS-PAGE, staining, and autoradiography. HC is an abbreviation for IgG heavy chain.

(E) Recombinant kinase was used to test GSK3β phosphorylation of ACF7(CT) and its different mutants in vitro. Phosphorylation of ACF7(CT) was detected by IB with Pi-Ser/Thr Ab.

exposing HF-SCs to different GSK3-specific inhibitors significantly increased the MT-binding affinity of endogenous ACF7 (Figure 3D). Together, these findings provided compelling support for GSK3β as an important regulator of ACF7's association with MTs and showed that GSK3β-mediated regulation was exerted exclusively at P1 and P2 of the ACF7's GSR domain.

The Wound-Healing Delay in ACF7-Deficient Skin Arises From Defective HF-SC Migration

Previously, we showed that mice targeted for loss of ACF7 in skin are defective in wound repair (Wu et al., 2008), a process known to involve HF-SCs (Ito et al., 2005; Tumbar et al., 2004). When coupled with the appearance of ACF7 on the list of genes upregulated in HF-SCs (Figure S1B) and an emerging role for Wnt signaling in wound repair (Fathke et al., 2006; Ito et al., 2007; Stoick-Cooper et al., 2007), our finding of GSK3β as a potential regulator of ACF7 took on newfound importance and merited further investigation.

To begin to evaluate how ACF7 functions in this pathway, we first purified HF-SCs (CD34^{hi}α6-integrin^{hi}) by fluorescence activated cell sorting (FACS) versus other basal cells (CD34^{neg}α6-integrin^{hi}) (Blanpain et al., 2004). RT-PCR and immunoblot on these purified cell populations verified ACF7's enrichment in HF-SCs at both mRNA and protein levels (Figure 4A). Immunofluorescence further documented elevated ACF7 in this niche throughout the hair cycle (Figure 4B).

Loss of ACF7 in HF-SCs did not alter bulge architecture (data not shown) nor did it affect expression of key bulge markers (Blanpain and Fuchs, 2009) (Figure 4C). In addition, no significant changes were found in proliferation or apoptosis of homeostatic HF-SCs (more details below) or in hair growth or cycling (Wu et al., 2008). We therefore focused on the hypothesis that the associated defects in wound repair originate from perturbations in HF-SC migration. To test this, we bred our ACF7$^{fl/fl}$ animals with mice expressing a progesterone-regulatable recombinase (*K15-Cre-PGR*) specifically in bulge SCs (Ito et al., 2005). To monitor HF-SC progeny in a wound response, we further bred these mice to *Rosa26-lox-Stop-lox-LacZ* reporter animals.

As expected, treatment of adult mice with RU486 (a progesterone antagonist) activated Cre and selectively marked HF-SCs. When challenged to a wound, activated LacZ+ bulge cells exited the niche and migrated upward to re-epithelialize wounded epidermis (Figure 4D). This was readily observed by whole-mount staining, which displayed trails of HF-SC-derived blue (LacZ+) cells emanating from perilesional follicles of wounded tissue (dashed arrows). By contrast, *ACF7* cKO bulge cells were delayed in this process by ~40% compared with WT controls over 4–6 days after injury (Figures 4D and 4E). Importantly, since targeting was specific to bulge cells, the delay was directly attributable to an SC defect. Moreover, ACF7-deficiency did not affect proliferation or apoptosis of bulge SCs, indicating that the defect was rooted in cell migration (Figures S3A and S3B).

To examine the contribution of GSK3β in this process, we took a pharmacological approach to manipulate GSK3β activity in vivo. Wounds on WT skin were treated with either lithium chloride (LiCl), which directly inhibits GSK3β, or wortmannin, which activates GSK3β by inhibiting an upstream regulator, phosphoinositol-3 kinase (PI3K). Interestingly, both treatments impaired wound-induced cell migration out of the adult HF-SC niche (Figure 4F), suggesting that spatiotemporal regulation of GSK3β's activity is required to achieve efficient bulge SC migration in vivo.

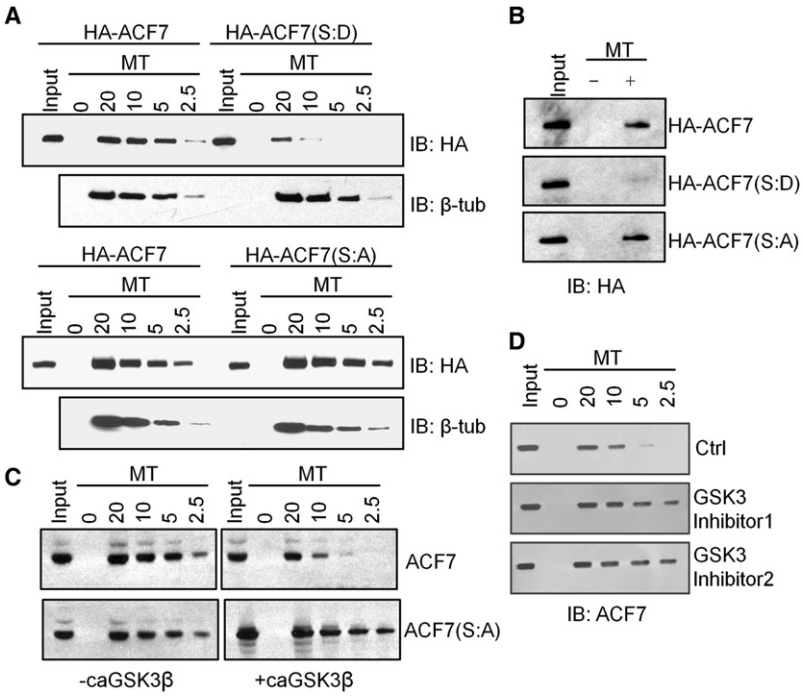

Figure 3. GSK3β Phosphorylation of ACF7's GSR Domain Inhibits Microtubule Binding

(A) In vitro binding assays on purified ACF7 proteins. After incubating with 0–20 μg taxol-stabilized MTs, purified WT, or mutant versions of full-length, HA-tagged ACF7 were cosedimented and subjected to IB analyses. Note that phosphomimetic S:D but not phosphorylation-refractile S:A ACF7 shows significantly reduced binding affinity.

(B) In vivo MT-binding assays. Lysates were prepared from cells expressing HA-tagged ACF7 or ACF7 mutants, and cosedimentation assays were performed as in (A).

(C) Lysates were prepared from cells coexpressing caGSK3 with HA-tagged ACF7 or ACF7(S:A). Cosedimentation assays and IBs were as in (A).

(D) Lysates were prepared from untreated cells or cells treated with GSK3β inhibitors (1: LiCl, 2: AR-A01448). Cosedimentation assays and IBs were as in (A). Figure 3 is associated with Figure S2.

The Polarization of MTs along Actin-Focal Adhesion Networks is Abrogated When ACF7 Is Phosphorylated by GSK3β

Previously, we showed that when *ACF7* is ablated, cultured epidermal keratinocytes cannot coordinate microtubule growth along F-actin filaments, a feature that in turn leads to overstabilization of focal adhesions (FAs) and defective cell movement (Wu et al., 2008). Based on our results thus far, we posited that in vivo, HF-SCs might respond to migratory stimulations such as Wnt signaling by spatiotemporally regulating ACF7-MT connections and promoting the cytoskeletal remodeling needed for polarized migration. To test this hypothesis, we first generated phospho-specific ACF7 Abs against two synthetic phospho-peptides corresponding to the ACF7 GSR sequences encompassing P1 and P2, respectively. Each Ab was specific for the phosphorylated state of its GSK3β target sequence: when ACF7 was not phosphorylated or when the sites were selectively mutated, the Abs failed to recognize the ACF7 protein (Figures S4A and S4B).

Isolated HF-SCs can sustain long-term culture without losing stemness (Blanpain et al., 2004), allowing us to investigate the role of ACF7 phosphorylation in vitro. Both ACF7 Abs detected the expected sized band in immunoblots of cultured bulge SC but not *ACF7* cKO lysates (Figure 5A). Importantly, these signals were sensitive not only to chemical inhibitors of GSK3β but also to recombinant Wnt3a. These data confirmed the specificity of our phospho-specific Abs and further demonstrated the ability of Wnt signaling to repress ACF7 phosphorylation in its C-terminal tail.

We next examined the GSK3β phosphorylation status of endogenous ACF7. In vitro, ACF7 decorated the ends of MTs that are coaligned with underlying F-actin cables (Figure 5B). By contrast, phospho-ACF7 was diffuse and/or punctate throughout the cytoplasm and showed no association with these MT cables (Figure 5C). Nevertheless this cytoplasmic staining was specific for ACF7, as it was abolished in *ACF7* KO bulge cells (Figure 5C). These findings were consistent with the phospho-dependent decreased affinity of ACF7 for MTs that we observed in vitro and revealed a marked correlation between GSK3β phosphorylation of ACF7 and a severing of the ACF7-MT connection.

To directly evaluate the effect of GSKβ phosphorylation on this process, we overexpressed caGSK3β in WT cultured bulge SCs. In contrast to empty vector alone (Figure 5D, left), caGSK3β dramatically reduced ACF7 localization along MTs (Figure 5D, center). Moreover, and quite remarkably, expression of constitutively active GSK3β transformed the straight and radial MTs of WT cells into a network of bent and curly MTs, reminiscent of the aberrant MT network typifying *ACF7* KO cells (Figure 5D, compare with data in Figure 5C).

If GSK3 activation and phosphorylation of ACF7 is responsible for severing the polarization of MTs at the migrating front, then inhibiting endogenous GSK3β activity might be expected to stabilize these connections. Indeed, when we treated HF-SCs with LiCl, under conditions that potently inhibited GSK3β activity and ACF7 phosphorylation, ACF7 clustered at the ends of MTs (Figures 5A and 5E). Additionally, polarized sites of converging ACF7, MT, and F-actin usually colabeled with Abs against FA proteins (Figure S4C).

ACF7-deficiency stabilizes FA through inhibiting MT targeting to FA (Wu et al., 2008). However, when DsRed-Zyxin-expressing HF-SCs were subjected to videomicroscopy and quantified, the effects of LiCl on FA turnover were modest (Figure S4D, Movie S1). This was also the case for the average size of FAs and the level of focal adhesion kinase (FAK) activity, which influence FA dynamics as well (Figures S4E and S4F). Overall, these results suggest that constitutive association between ACF7 and MTs may not elicit the alterations in FA stability that are seen when ACF7 is missing altogether.

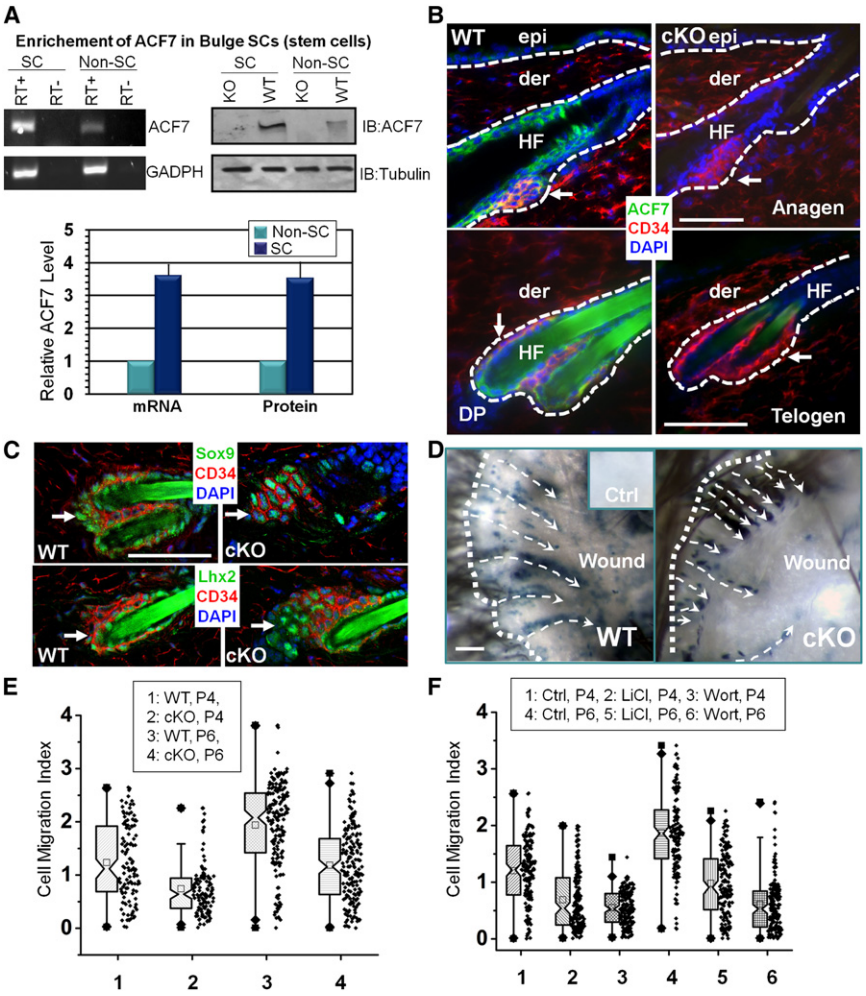

Figure 4. Loss of ACF7 Impairs Migration of Bulge Stem Cells In Vivo and In Vitro

(A) RT-PCR (upper left), IB (upper right) and quantifications (lower) of ACF7 mRNA (real-time RT-PCR) and protein from isolated bulge HF-SCs and non-SC extracts. Error bars denote standard deviation (SD).

(B) Immunofluorescence of skin sections at different hair cycle stages. ACF7 is enriched in bulge (arrows), and although CD34 is present in dermis, its epithelial expression is specific to bulge. Color coding is according to secondary Abs used in detection. Nuclei were counterstained with DAPI (blue). Dashed lines denote basement membrane. The following abbreviations are used: HF, hair follicle; der, dermis; epi, epidermis; DP, dermal papilla. The scale bars indicate 50 μm.

(C) Immunofluorescence of sections of HF bulges (arrows) for SC markers indicated.

(D and E) Whole-mount LacZ imaging and quantifications of bulge SCs and their progeny from perilesional follicles of WT and *ACF7 cKO* mice. Dashed lines denote wound boundary; dashed arrows denote trails of bulge SCs and progeny that migrated into wound. The inset is of unwounded K15-Cre-activated skin where LacZ expression is confined to the bulge, not visible on the body surface. Blue cells migrated upward only after wounding. The length of the blue cell trails 4 or 6 days after wounding (P4 and P6) was quantified in (E) by box-whisker plots.

(F) Wounded animals were topically treated with LiCl or wortmannin (Wort). Bulge SC migration was quantified as in (E). Figure 4 is associated with Figures S1 and S3.

GSK3β has many targets, which complicates the interpretation of LiCl experiments (Sun et al., 2009). To distinguish the specific effects of GSK3β on ACF7-mediated cytoskeletal dynamics, we performed rescue experiments with our ACF7 phosphorylation mutants. To more precisely control concentration and ensure comparable expression of encoded proteins, we microinjected our expression constructs into primary cultured HF-SCs null for *ACF7*.

Introducing GFP-tagged versions of either full-length or S:A mutant ACF7 restored ACF7's localization to the MT ends residing near or at the cortex (Figure 5F). Consistent with their MT-binding capability, kinase-refractile ACF7(S:A) and full-length ACF7 also generated arrays of radial MT trajectories in individual *ACF7* null cells (Figure 5F). By contrast, the phosphomimetic ACF7(S:D) was diffusely localized, and its MT organization appeared no different than in uninjected or GFP-injected *ACF7* null cells (Figure 5F). Taken together, these experiments provide compelling evidence that GSK3β plays a critical role in regulating ACF7's dissociation from MTs and that phosphorylation is sufficient to dramatically alter polarized organization of MTs along actin stress fibers converging at FAs.

GSK3β Phosphorylation of ACF7 Must Be Dynamic to Govern Polarization and Directed Movement in Cultured HF-SCs

Cultured HF-SCs further allowed us to examine their directional movement in vitro. When subjected to a modified Boyden chamber assay with conditioned feeder fibroblast medium as a chemo-attractant, WT HF-SCs showed a marked, dose-dependent migratory response, which was greatly diminished in HF-SCs lacking ACF7 (Figure 6A). Moreover, stimulation of WT HF-SCs' migration was achieved only when conditioned medium was administered in a positive concentration gradient. These data further documented the chemotactic nature of the response, and confirmed ACF7's role in sustaining directional cell movement. Consistent with our in vivo observations, treatment of HF-SCs with GSK3β inhibitors or ectopic expression of caGSK3β inhibited the response (Figure 6B).

Directionality of movement relies heavily on cell polarity, and prior studies indicated that embryonic endodermal cells lacking ACF7 cannot sustain cell polarity after scratch-wounding in vitro (Kodama et al., 2003). To evaluate how regulated ACF7-MT connections might contribute to cell polarity, we devised

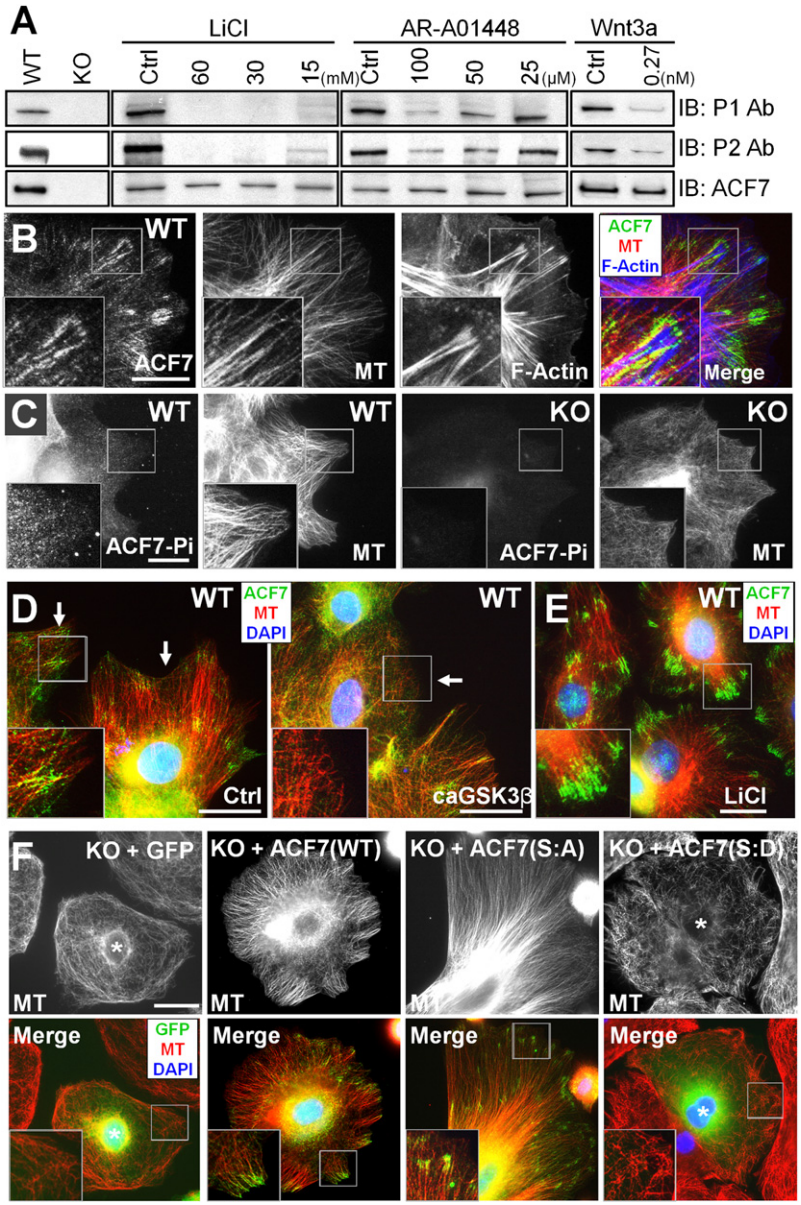

Figure 5. ACF7 Is Required to Polarize MTs along F-Actin-Focal Adhesion Networks, which in Turn Are Inhibited by GSK3β Activity

(A) ACF7 protein and its phosphorylation status were evaluated by immunoblot of lysates from KO or WT bulge SCs treated with GSK3β inhibitors or Wnt3a, as indicated.

(B and C) Cultured bulge SCs immunolocalized for α-tubulin (MT), ACF7, ACF7 phosphorylation (ACF7-Pi, with P2-specific Abs), or F-actin (phalloidin). Notes: (1) ACF7 but not phospho-ACF7 is enriched at polarized MT tips and (2) the diffuse cytoplasmic ACF7-Pi pattern of WT is absent in KO cells.

(D) Immunofluorescence of WT bulge SCs expressing caGSK3β or vector control. Transfected cells are marked with arrows. Note: caGSK3β inhibits ACF7 localization at MT tips and leads to disorganized MT networks.

(E) WT bulge cells were treated with LiCl to impair GSK3β activity and subjected to immunofluorescence as indicated. Note clusters of ACF7 at cell periphery.

(F) Cultured *ACF7* KO bulge SCs were microinjected with expression vectors encoding GFP alone, GFP-ACF7 (rescue), GFP-ACF7(S:A) (GSK3-refractile), or GFP-ACF7 (S:D) (phosphomimetic). Cells were immunolabeled for MTs. Note that only WT and S:A mutant, and not GFP or S:D mutant, localized and rescued MT organization defects that occur in KO bulge SCs in low-Ca^{2+} medium. Wherever the field includes uninjected cells, injected ones are denoted by an asterisk.

For (B–F), boxed areas are magnified in insets. The scale bars represent 20 μm. Figure 5 is associated with Figure S4.

a method to polarize cultured bulge SCs by seeding them at low density on fibronectin-coated dishes and then elevating Ca^{2+} levels to induce cell-cell adhesion. Under these conditions, the perimeter of isolated WT colonies exhibited significant polarity as determined by immunolocalization of phosphorylated (inactive) GSK3β, Par proteins, and aPKC (Figure 6C, and Figure S4G). Polarization of perinuclear Golgi was particularly prominent, enabling quantification by measuring its preferential localization around the axis bisecting nucleus and colony edge. Interestingly, ACF7-deficient bulge SCs displayed polarized GSK3β phosphorylation but not Golgi (Figure 6C). Moreover, manipulating GSK3β activity in WT HF-SCs disrupted Golgi polarization (Figure 6D). These data placed ACF7 midstream in the pathway that links polarized GSK3β inhibition at the HF-SC front and Golgi polarization in the perinuclear region.

Our findings were intriguing in light of prior data showing that MTs are essential for polarizing Golgi assembly (Miller et al., 2009; Siegrist and Doe, 2007). We therefore wondered whether rescuing the ability of MTs to polarize along actin cables might also rescue defective Golgi polarization. To test this possibility, we repeated the polarization assays, this time with bulge SCs microinjected with our GFP-tagged versions of WT and phosphorylation-altered ACF7. WT-ACF7 rescued polarization of HF-SCs (Figure 6D). As expected from its failure to bind MTs (Figure 5F), ACF7(S:D) also failed to effectively polarize Golgi (Figure 6D). Interestingly, however, even though ACF7(S:A) efficiently rescued MT organization (Figure 5F), it failed to rescue Golgi orientation (Figure 6D).

Finally, we tested the ability of our mutants to rescue the chemotactic migration defects seen in *ACF7* null cells. As shown in Figure 6E, only WT-ACF7 rescued the ability of bulge SCs to migrate efficiently. Together, these data showed that the ability of MTs to track along actin cables is not sufficient to achieve either polarization or effective migration of bulge SCs. Moreover, both of these processes require in addition the dynamic regulation of ACF7 phosphorylation since neither the phosphomimetic mutant, the phosphorylation refractile mutant, nor the two

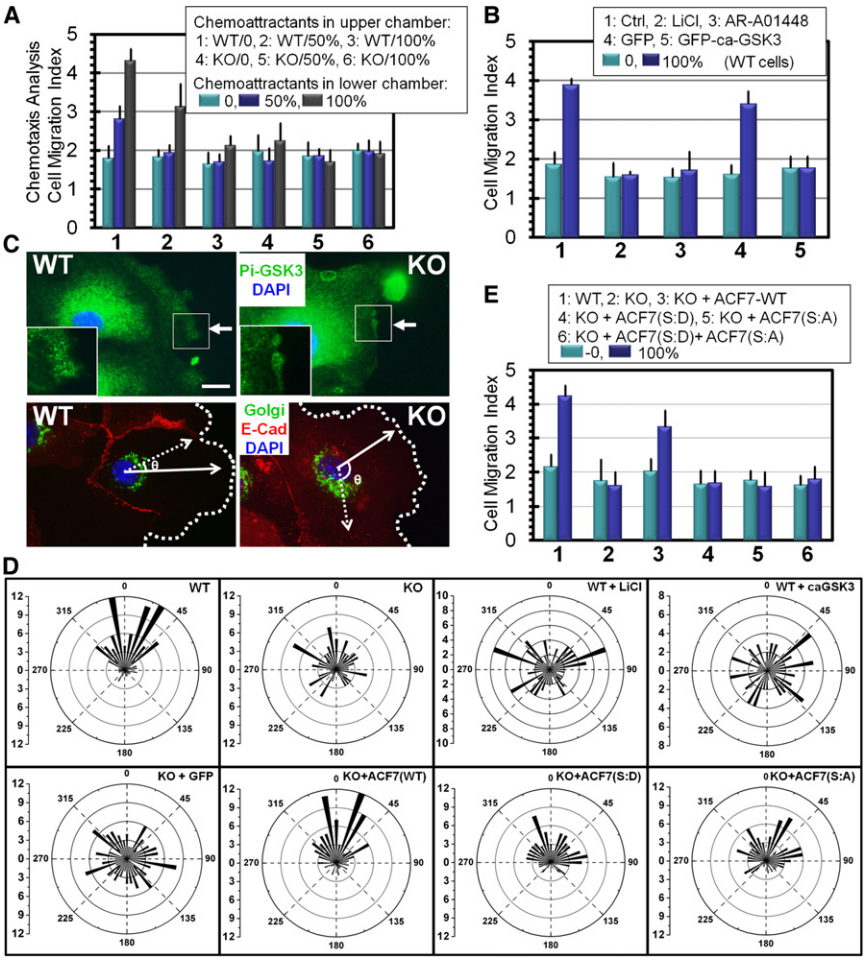

Figure 6. GSK3β Phosphorylation Governs ACF7 Functionality in Cell Polarity and Directional Cell Movement in Vitro

(A) Isolated HF-SCs were subjected to modified Boyden chamber assays, and a checkerboard analysis was performed to distinguish chemokinesis versus chemotaxis effects. Feeder-conditioned medium was used as chemoattractant and was mixed with serum-free medium to load into upper and lower chambers. Migration was quantified as in Experimental Procedures, and presented as bar graphs. Color coding corresponds to the concentration of chemoattractants in the lower chamber. Concentrations of chemoattractants in upper chamber are indicated in bar graph legends. Note that only WT cells showed significant chemotactic behavior when exposed to a positive chemoattractant gradient.

(B) Migration of treated or transfected WT HF-SCs was examined as in (A), with only 0 or 100% of chemoattractants used in lower chamber and no chemoattractants in upper chamber. Note that both global inhibition and artificial activation of GSK3β activity inhibit migration of HF-SCs.

(C) Immunofluorescence detects Ser-9 GSK3β phosphorylation (inactivation), GM-130 (Golgi), E-cadherin (E-Cad), and chromatin (DAPI). Arrows denote enriched phospho-GSK3β at the leading edge. Dashed lines denote colony perimeters. θ represents angle between solid arrow, denoting outward direction of HF-SC colony and dashed arrow, denoting Golgi orientation. Note polarization of inactivated GSK3β at migrating edge of both WT and *ACF7* null HF-SCs, and loss of Golgi polarization in *ACF7* null HF-SCs. The scale bar represents 20 μm.

(D) Windrose plots of Golgi orientation (quantification of angle θ) in treated or untreated WT and microinjected or uninjected ACF7-deficient cells. Note random distribution of θ in KO cells; only WT ACF7 restores proper cell polarity.

(E) Quantifications of chemotactic behaviors show that only WT ACF7 rescues migration defects in *ACF7* null bulge SCs. Error bars represent SD.

mutants combined (Figure 6E) were able to rescue these defects in KO cells.

GSK3β Phosphorylation of ACF7 Regulates Bulge SC Migration and Skin Wound Repair In Vivo

We next focused on whether dynamic regulation of ACF7 phosphorylation coordinates polarized bulge SC migration during wound repair in vivo. We began by engineering transgenic mice expressing N-terminally GFP-tagged, full-length versions of ACF7 and ACF7 S:A under the control of K14 promoter and enhancer. Mice genotypic for *K14-ACF7* or *K14-ACF7(S:A)* alleles were born in the expected Mendelian numbers and grew normally (Figure S5A). Transgenic ACF7 and ACF7(S:A) GFP-tagged proteins of the correct size were expressed comparably and exhibited the expected differential GSK3β phosphorylation states in vivo (Figure S5A). Immunofluorescence confirmed skin-specific transgene expression (Figure S5B).

To determine the ability of these transgenic proteins to compensate for loss of ACF7 in HF-SCs in vivo, we bred our transgenics to *ACF7$^{fl/fl}$:K15-Cre-PGR:Rosa26-LacZ* mice and then induced ablation of endogenous *ACF7*. Mice expressing these transgenes and not ACF7 in their HF-SCs were visibly normal, and no gross differences were noted in hair cycles (Figure S5C; data not shown). Immunofluorescence for a variety of differentiation markers showed normal morphology and localization patterns (Figures S5D and S5E).

Given the normal tissue architecture and homeostasis, we next turned to investigating how ACF7's GSK3β-phophorylation status affects the ability of HF-SCs to respond and migrate outward to repair epidermis upon skin wounding. In response to punch wounds, only *ACF7* cKO mice expressing GFP-ACF7, and not GFP-ACF7(S:A), showed significant rescue of bulge SC migration defects, as measured by LacZ whole-mount staining (Figure 7A, left). This difference appeared to reflect a differential ability to restore directional cell movement, since bulge SC proliferation and apoptosis assays showed no change (Figures S3A and S3B). Although most data shown are for *K15-Cre-PGR*, similar results were obtained when the wounding challenge was

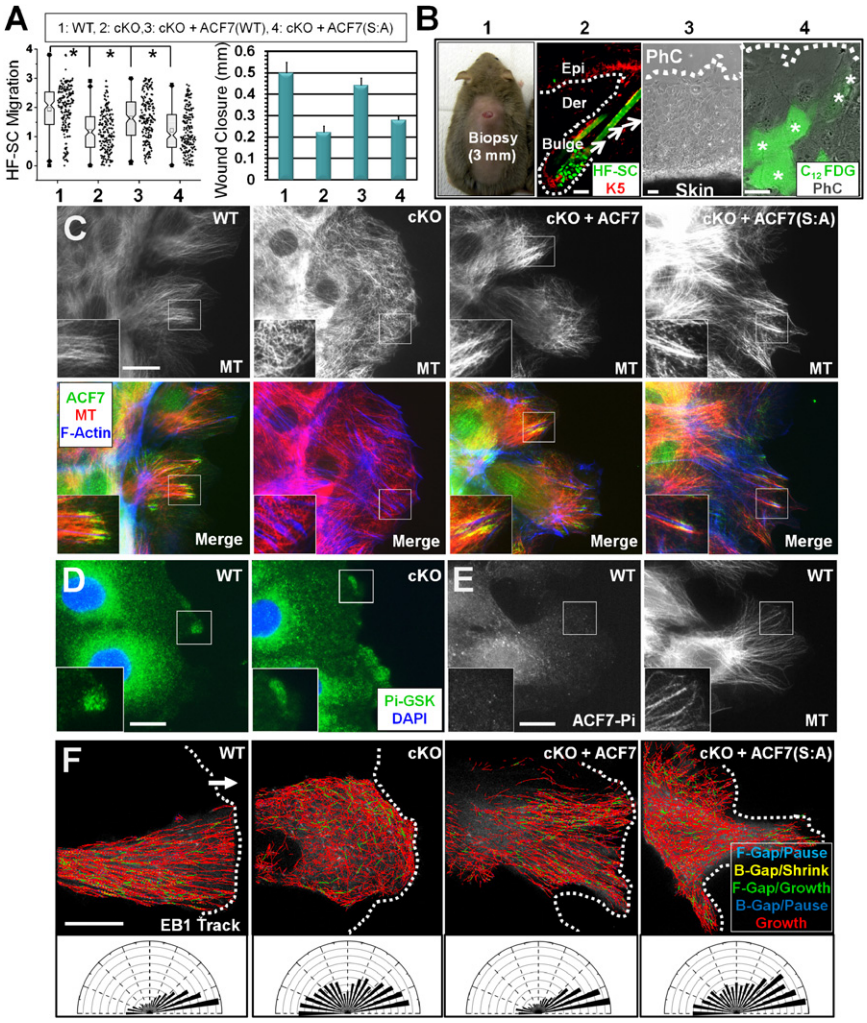

Figure 7. GSK3β Phosphorylation of ACF7 Plays a Critical Role in Bulge Stem Cell Migration and Skin Wound Repair In Vivo

(A) Box and whisker plots (left) and bar graphs (right) show that in vivo migration of HF-SCs and overall skin healing (length of hyperproliferative epithelium in wound) were restored by WT-ACF7 transgene but not ACF7(S:A). Stars (★) represent p value less than 0.05, and error bars represent SE.

(B) Outline of methodology used to activate and induce migration of quiescent HF-SCs in skin biopsy (1) by ex vivo wounding. A typical telogen HF is shown in (2) with arrows marking potential direction of HF-SC migration upon wounding. HF-SCs are identified by C12-FDG (a fluorogenic substrate of LacZ), and outward migration is visualized by phase contrast (PhC) or fluorescence microscopy. Dashed lines denote basement membrane in (2), or migrating front in (3–4). Stars denote C_{12}FDG(+) cell in (4).

(C) Representative examples of SC progeny after exiting and migrating out of the HF bulge. Immunofluorescence was used to visualize ACF7, MT, and F-actin. Boxed areas are magnified as insets.

(D–E) Cells migrating out of the bulge SC niche were immunostained for phospho-GSK3β and phospho-ACF7. Note enrichment of inactive (phosphor) GSK3β at migrating front and corresponding lack of GSK3β-phosphorylation of ACF7 at plus ends of MTs localized there.

(F) Live imaging of progeny that migrated out of the bulge SC niche during wound response. Cells were microinjected to express GFP-EB1, and MT +tip movements were then monitored by videomicroscopy and tracked automatically (upper). Corresponding MT behavior is color-coded and described in text and Experimental Procedures. Data for directionalities of MT growth were collected from movies and then quantified and presented as Windrose plots (lower). Arrow denotes direction toward wound front. Dotted lines denote migrating front of cells streaming from the wound-induced skin explant. The scale bar represents 20 μm. Figure 7 is associated with Figures S5 and S6.

broadened by using transgenic mice mated to *ACF7$^{fl/fl}$: K14-Cre* mice. Once again, the area of hyperproliferative epithelium that typically migrates into the wound site was only significantly rescued by GFP-ACF7 and not GFP-ACF7(S:A) (Figure 7A, right).

Finally we addressed whether changes in GSK3β activity alter ACF7's ability to coordinate actin- MT dynamics during wound-induced directed migration of bulge SCs out of HFs. For this purpose, we induced a rapid wound response in HFs by cutting the skin at the resting (telogen) phase and placing it into rich medium. In a process analogous to wound healing, the outward migration of activated HF-SC progeny could then be imaged by videomicroscopy and immunofluorescence (Figures 7B–7F and Figure S6).

Targeted bulge cell progeny were identified by their ability to cleave a fluorogenic substrate for LacZ (Figure 7B). Consistent with our in vitro results, Golgi complex as well as Par6 and aPKC localized in a polarized fashion in WT bulge SCs at the leading front (Figure S6A). These cells also contained FAs (Figure S6A) and well-polarized MT bundles that coaligned with F-actin, and ACF7 localized at the interface between these MT +tips and F-actin bundles (Figure 7C). Loss of ACF7 resulted in disorganized MT architecture (Figure 7C). Additionally, ACF7 deficiency or change in GSK3β activity led to perturbations in cell polarity and migration of the marked bulge SCs/progeny that were streaming from the HFs. Interestingly, while both WT and S:A mutant ACF7 rescued the disorganized MT network, only WT ACF7 rescued alterations in cell polarity and migration (Figure 7C and Figures S6B and S6C).

Similar to our in vitro results (see Figure 6C) and those obtained from other model systems (Sun et al., 2009), Ser9-phosphorylated (inactive) GSK3β was enriched at the leading edge of migrating HF-SCs (Figure 7D). Consistent with these data, the majority of ACF7 phosphorylated by GSK3β was localized in the cell body and not at the leading edge of HF-SCs (Figure 7E).

As a +tip protein, ACF7 can guide movement of MT plus ends. To monitor potential polarity of MT dynamics during wound-induced migration, we microinjected migrating bulge SCs/progeny with a GFP-tagged EB1 expression vector. Videomicroscopy combined with automated tracking of this plus end (+tip) MT-binding protein revealed polarized MT growth toward the migrating front of WT HF-SCs (Movies 2 and Figure 7F). Directionality of MT growth was largely randomized in KO cells, and only WT-ACF7, and not ACF7(S:A), rescued it (Figure 7F). Taken together, these findings underscore an essential physiological role for GSK3β-mediated phosphorylation of ACF7 in sustaining polarized MT growth and directed HF-SC migration during wound healing.

DISCUSSION

Aberrant mobilization of SCs in response to injury can delay wound repair and have dire consequences to animal survival (Fuchs, 2009). Exposed to frequent mechanical stresses, skin SCs have developed a unique and elaborate cytoskeletal system. However little is known about how cytoskeletal dynamics are coordinated in these or other SCs. In this report, we've demonstrated the role of ACF7 and ACF7-mediated cytoskeletal dynamics in SCs in vivo. Our studies show that ACF7 is required for efficient upward migration of bulge cells in response to wounding and that this function is primarily rooted in ACF7's ability to coordinate MT dynamics and polarize HF-SCs. Through a comprehensive approach encompassing biochemistry and molecular and cell biology, we further unveiled a hitherto unrecognized regulatory role for GSK3β-mediated phosphorylation of ACF7's major MT-binding domain. We show that the consequence of this phosphorylation is the attenuation of interactions between ACF7's basic GSR domain and the acidic C-terminal tubulin tails.

Polarized cell movement is an essential component of diverse biological processes such as cancer metastasis, tissue development, and wound healing (Lauffenburger and Horwitz, 1996). All these processes share significant similarities regarding their mechanisms for sensing directional cues and translating them into directional locomotion. Cells under the influence of various chemotactic molecules exhibit polarized activation of signaling proteins, such as the CDC42 Rho GTPase and PI3K, that guide differential remodeling of cytoskeletons at the leading edge versus the back of cells (Etienne-Manneville, 2004; Siegrist and Doe, 2007).

MTs play a particularly important role in this process, delivering positional information to establish the proper site of cortical polarity (Siegrist and Doe, 2007). Once MTs and their associated proteins determine the polarity site, a positive feedback loop initiates interactions between the actin-rich cortex and growing (plus) ends of MTs, resulting in reinforcement and maintenance of polarity. Such a mechanism not only provides cells with the ability to sense and amplify small asymmetries in their field but also buffers and maintains the polarity axis after it is established. Common components of MT-based polarity pathways are plus-end-directed kinesin motors and MT plus-end-stabilizing proteins, including CLIP-170, EB1, Clasps, and adenomatous polyposis coli (APC) (Akhmanova and Steinmetz, 2008). Our prior studies added ACF7 to this list (Karakesisoglou et al., 2000; Kodama et al., 2003; Wu et al., 2008). Our current study lends physiological relevance for ACF7's ability to polarize MTs and identifies a specific role for this connection in enabling HF-SCs to polarize and migrate into a wound site. In addition, our results elucidate a hitherto unappreciated signaling pathway whereby ACF7's function is regulated dynamically in HF-SCs by GSK3β in order to control the directionality of MT growth, cell polarity, and migration.

GSK3β modifies various regulatory components of MT cytoskeletons, including APC and some neuronal MT-associated proteins (Sun et al., 2009). Intriguingly, a recent study showed that ErbB2-induced repression of GSK3 is required for MT capture and targeting of ACF7 to plasma membrane in breast carcinoma cells (Zaoui et al., 2010). Our results identify ACF7 as a GSK3β substrate in skin somatic SCs and raise the possibility that GSK3β may function as a master regulator of MT polarity. Importantly, however, our findings reveal that although only phosphomimetic ACF7 mutants disrupt MT organization, nonphosphorylatable ACF7 mutants nonetheless impair global cell polarization and SC migration. These findings underscore the importance of regulating ACF7's phosphorylation status in a spatially and temporally defined manner in order to establish proper directionality in cells.

Consistent with this notion, GSK3β activity is specifically inhibited by CDC42 signaling at the leading edge of migrating cells (Etienne-Manneville and Hall, 2003; Sun et al., 2009) and also by Wnt signaling, which is often polarized in tissues (Nusse, 2008). Notably, Wnts have been broadly implicated in wound repair and are required for HF-SC activation at the start of the hair cycle (Blanpain and Fuchs, 2009). Although ACF7 has been implicated in recruiting the Axin-APC-GSK3β complex to the site of active Wnt signaling in the gastrulating embryo (Chen et al., 2006), an essential role in Wnt signaling would not explain why SC activation and hair cycling still occur in *ACF7* cKO skin. Our findings now provide an alternative role for ACF7 in Wnt signaling, namely as a downstream sensor of GSK3β inhibition and a mobilizer of the polarized response necessary for SC migration. Collectively, our findings support a model in which upstream chemotactic cues, e.g., Wnt signaling, trigger cellular polarization, and directional movement through spatiotemporal regulation of ACF7 phosphorylation by GSK3β (Figure S7). In this model, some outcomes of Wnt signaling and GSK3β inhibition, e.g., SC activation, proliferation, and fate commitment in normal homeostasis, might still be maintained while others, e.g., SC migration during wound repair, would rely upon the ability to polarize directed migration. Future studies will determine the extent to which this pathway can explain ACF7's broad and essential presence in tissues.

In closing, our findings provide insights into the complex but important molecular machinery underlying the polarized SC migration that integrates injury-induced migratory signals, cytoskeletal remodeling, and polarized cell movements in HF-SCs. Our studies also add to the repertoire of spectraplakin's many diverse and critical functions and now pave the way for probing more deeply into the role of spectraplakins in mammalian SCs.

EXPERIMENTAL PROCEDURES

Generation of Transgenic Mice and Skin Wound Healing

The transgenic expression cassette was constructed so that GFP-ACF7 or GFP-ACF7(S:A) cDNA sequence was inserted 3′ to the human K14 promoter and enhancer and β-globin 5′UTR, and 5′ to the K14 3′UTR. Mice harboring these transgenes were engineered in Fvb/n albino mice and selected for their comparable expression relative to endogenous ACF7.

Skin-wound-healing assays were performed as described (Wu et al., 2008). To monitor the migration of SCs and their progeny after wounding, we treated *K15-Cre-PGR:R26-LacZ:ACF7$^{fl/fl}$* mice ± transgene with RU486 for 5 days starting at their first telogen (∼P21). At 8 weeks, mice were anesthetized and full-thickness punch wounds (6 mm) were introduced on their backs. Skin samples were then collected at 4 or 6 days after wounding and β-galactosidase activity was detected in whole-mount tissues by X-gal staining (Ito et al., 2005). For each genotype, at least ten mice were analyzed for the wound response.

To monitor the activation and migration of SCs from resting HFs subjected to wound response, we took 3 mm biopsies from back skin of 2-month-old *K15-Cre-PGR:R26-LacZ* mice that were treated with RU486. Biopsies were coated with a thin layer of matrigel for adhesion and immediately transferred to a coverslip coated with 10 μg/ml fibronectin. Skins were then incubated at room temperature for 10 min to solidify the matrigel and then exposed to rich E-media containing 15% serum and 0.3 mM calcium (Blanpain et al., 2004), which promoted HF-SC outgrowth within 2–3 days, analogous to a wound response. Live HF-SCs and progeny were identified with fluorogenic β-galactosidase substrates C_{12}FDG or C_{12}RG (Invitrogen, yield green or red fluorescence respectively) according to the manufacturer's instruction.

Cell Migration Assays and Time-Lapse Videomicroscopy

Migration assays in 96-well chemotaxis chambers (Millipore, Billerica, MA) were carried out according to manufacturer's instructions. Briefly, 3T3 fibroblast-conditioned medium or serum-free medium (control) was added to the lower chamber. Bulge SCs were added to the upper chamber, and, after 10 hr at 37°C, cells that migrated through the filter into the bottom chamber were collected, lysed, and stained with CyQuant GR dye (labels DNA). A fluorescence plate reader was used to quantify fluorescence intensities.

To track individual HF-SC movement, skin biopsies were imaged with an Olympus phase contrast microscope for 1 day and manually tracked with National Institutes of Health's ImageJ. Displacements along the direction facing the leading edge of the migrating front were recorded and quantified (Wu et al., 2008). To monitor MT plus end movement in live cells, we microinjected HF-SCs with plasmid encoding GFP-EB1. Six hours after injection, cells were imaged with a confocal spinning-disk microscope (Wu et al., 2008) for 5 min at 2 s/frame. Plus Tip Tracker software package (Matov et al., 2010) was used to process and track EB1 movements at the leading front. Because of MT dynamic instability, some gaps appeared between MT growth (red solid tracks in the output image of Figure 7F). Gaps could occur in either the forward or backward direction depending on underlying MT dynamics and detection performance. Forward gaps could be a MT pause (cyan dotted) or reclassified as growth (green solid). Backward gaps could be MT shrinkage/catastrophe (yellow dotted) or reclassified as pause events (blue dotted). The same color codes were used in the output movie (Movie S2), and initiation of a new growth track or gap was marked by a circle with corresponding color. Angles between MT growth track and outward direction of explants were calculated with a linear fit function of Matlab and plotted as Windrose plots.

Microtubule Cosedimentation Assay, Subtilisin Treatment, and Immunoblotting

MT-binding assays were performed as described (Wu et al., 2008). Equivalent amounts of pellet were analyzed by CB staining or immunoblotting. Cleavage of the unstructured tubulin C terminus was carried out by limited proteolysis of taxol-stabilized MTs with subtilisin (Knipling et al., 1999). The proteolysis reaction was stopped by adding freshly prepared 20 mM PMSF in DMSO. Subtilisin-treated MTs were pelleted by ultracentrifugation at 60,000 × *g* and resuspended in MT-stabilizing buffer containing 20 mM PMSF and taxol to ensure complete removal of active protease and cleaved C-terminal tubulin fragments. Immunoprecipitations and immunoblotting were performed as described (Wu et al., 2004).

SUPPLEMENTAL INFORMATION

Supplemental Information includes Supplemental Experimental Procedures, seven figures, and two movies and can be found with this article online at doi:10.1016/j.cell.2010.12.033.

ACKNOWLEDGMENTS

We are grateful to M. Schober, Y.C. Hsu, E. Ezratty, and T. Chen for discussions and helpful comments and to J. Fernandez and H. Deng (Proteomics Center) for their technical assistance in mass spectrometry analysis. Valuable technical assistance was provided by N. Stokes, L. Polak, E. Wong, M Nikolova, J. Racelis, A. North, and S. Bhuvanendran. All mice used in this study were bred and maintained at the Rockefeller University Association for Assessment and Accreditation of Laboratory Animal Care International-accredited Comparative Biology Center (CBC) in accordance with institutional and National Institutes of Health guidelines. This work was supported by Grant R01-AR27883 from the National Institutes of Health. E.F. is an investigator of the Howard Hughes Medical Institute. X.W. was an American Association for Cancer Research Anna D. Barker Fellow in Basic Cancer Research and the recipient of a postdoctoral fellowship from the Jane Coffin Childs Memorial Fund for Medical Research.

Received: January 8, 2010
Revised: November 1, 2010
Accepted: December 17, 2010
Published: February 3, 2011

REFERENCES

Akhmanova, A., and Steinmetz, M.O. (2008). Tracking the ends: a dynamic protein network controls the fate of microtubule tips. Nat. Rev. Mol. Cell Biol. *9*, 309–322.

Blanpain, C., and Fuchs, E. (2009). Epidermal homeostasis: a balancing act of stem cells in the skin. Nat. Rev. Mol. Cell Biol. *10*, 207–217.

Blanpain, C., Lowry, W.E., Geoghegan, A., Polak, L., and Fuchs, E. (2004). Self-renewal, multipotency, and the existence of two cell populations within an epithelial stem cell niche. Cell *118*, 635–648.

Chen, H.J., Lin, C.M., Lin, C.S., Perez-Olle, R., Leung, C.L., and Liem, R.K. (2006). The role of microtubule actin cross-linking factor 1 (MACF1) in the Wnt signaling pathway. Genes Dev. *20*, 1933–1945.

Etienne-Manneville, S. (2004). Cdc42—the centre of polarity. J. Cell Sci. *117*, 1291–1300.

Etienne-Manneville, S., and Hall, A. (2003). Cdc42 regulates GSK-3beta and adenomatous polyposis coli to control cell polarity. Nature *421*, 753–756.

Fathke, C., Wilson, L., Shah, K., Kim, B., Hocking, A., Moon, R., and Isik, F. (2006). Wnt signaling induces epithelial differentiation during cutaneous wound healing. BMC Cell Biol. *7*, 4.

Fuchs, E. (2009). The tortoise and the hair: slow-cycling cells in the stem cell race. Cell *137*, 811–819.

Goryunov, D., He, C.Z., Lin, C.S., Leung, C.L., and Liem, R.K. (2010). Nervous-tissue-specific elimination of microtubule-actin crosslinking factor 1a results in multiple developmental defects in the mouse brain. Mol. Cell. Neurosci. *44*, 1–14.

Greco, V., Chen, T., Rendl, M., Schober, M., Pasolli, H.A., Stokes, N., Dela Cruz-Racelis, J., and Fuchs, E. (2009). A two-step mechanism for stem cell activation during hair regeneration. Cell Stem Cell *4*, 155–169.

Ito, M., Liu, Y., Yang, Z., Nguyen, J., Liang, F., Morris, R.J., and Cotsarelis, G. (2005). Stem cells in the hair follicle bulge contribute to wound repair but not to homeostasis of the epidermis. Nat. Med. *11*, 1351–1354.

Ito, M., Yang, Z., Andl, T., Cui, C., Kim, N., Millar, S.E., and Cotsarelis, G. (2007). Wnt-dependent de novo hair follicle regeneration in adult mouse skin after wounding. Nature *447*, 316–320.

Jefferson, J.J., Leung, C.L., and Liem, R.K. (2004). Plakins: goliaths that link cell junctions and the cytoskeleton. Nat. Rev. Mol. Cell Biol. *5*, 542–553.

Karakesisoglou, I., Yang, Y., and Fuchs, E. (2000). An epidermal plakin that integrates actin and microtubule networks at cellular junctions. J. Cell Biol. *149*, 195–208.

Knipling, L., Hwang, J., and Wolff, J. (1999). Preparation and properties of pure tubulin S. Cell Motil. Cytoskeleton *43*, 63–71.

Kodama, A., Karakesisoglou, I., Wong, E., Vaezi, A., and Fuchs, E. (2003). ACF7: an essential integrator of microtubule dynamics. Cell *115*, 343–354.

Lauffenburger, D.A., and Horwitz, A.F. (1996). Cell migration: a physically integrated molecular process. Cell *84*, 359–369.

Matov, A., Applegate, K., Kumar, P., Thoma, C., Krek, W., Danuser, G., and Wittmann, T. (2010). Analysis of microtubule dynamic instability using a plus-end growth marker. Nat. Methods *7*, 761–768.

Miller, P.M., Folkmann, A.W., Maia, A.R., Efimova, N., Efimov, A., and Kaverina, I. (2009). Golgi-derived CLASP-dependent microtubules control Golgi organization and polarized trafficking in motile cells. Nat. Cell Biol. *11*, 1069–1080.

Morris, R.J., Liu, Y., Marles, L., Yang, Z., Trempus, C., Li, S., Lin, J.S., Sawicki, J.A., and Cotsarelis, G. (2004). Capturing and profiling adult hair follicle stem cells. Nat. Biotechnol. *22*, 411–417.

Nusse, R. (2008). Wnt signaling and stem cell control. Cell Res. *18*, 523–527.

Nusse, R., Fuerer, C., Ching, W., Harnish, K., Logan, C., Zeng, A., ten Berge, D., and Kalani, Y. (2008). Wnt signaling and stem cell control. Cold Spring Harb. Symp. Quant. Biol. *73*, 59–66.

Obenauer, J.C., Cantley, L.C., and Yaffe, M.B. (2003). Scansite 2.0: Proteome-wide prediction of cell signaling interactions using short sequence motifs. Nucleic Acids Res. *31*, 3635–3641.

Rodriguez, O.C., Schaefer, A.W., Mandato, C.A., Forscher, P., Bement, W.M., and Waterman-Storer, C.M. (2003). Conserved microtubule-actin interactions in cell movement and morphogenesis. Nat. Cell Biol. *5*, 599–609.

Röper, K., Gregory, S.L., and Brown, N.H. (2002). The 'spectraplakins': cytoskeletal giants with characteristics of both spectrin and plakin families. J. Cell Sci. *115*, 4215–4225.

Schiller, M.R. (2007). Minimotif miner: A computational tool to investigate protein function, disease, and genetic diversity. Curr Protoc Protein Sci, *2* 10.1002/0471140864.ps0212s48, Unit 2.12.

Siegrist, S.E., and Doe, C.Q. (2007). Microtubule-induced cortical cell polarity. Genes Dev. *21*, 483–496.

Stoick-Cooper, C.L., Weidinger, G., Riehle, K.J., Hubbert, C., Major, M.B., Fausto, N., and Moon, R.T. (2007). Distinct Wnt signaling pathways have opposing roles in appendage regeneration. Development *134*, 479–489.

Sun, D., Leung, C.L., and Liem, R.K. (2001). Characterization of the microtubule binding domain of microtubule actin crosslinking factor (MACF): identification of a novel group of microtubule associated proteins. J. Cell Sci. *114*, 161–172.

Sun, T., Rodriguez, M., and Kim, L. (2009). Glycogen synthase kinase 3 in the world of cell migration. Dev. Growth Differ. *51*, 735–742.

Tumbar, T., Guasch, G., Greco, V., Blanpain, C., Lowry, W.E., Rendl, M., and Fuchs, E. (2004). Defining the epithelial stem cell niche in skin. Science *303*, 359–363.

Wu, X., Suetsugu, S., Cooper, L.A., Takenawa, T., and Guan, J.L. (2004). Focal adhesion kinase regulation of N-WASP subcellular localization and function. J. Biol. Chem. *279*, 9565–9576.

Wu, X., Kodama, A., and Fuchs, E. (2008). ACF7 regulates cytoskeletal-focal adhesion dynamics and migration and has ATPase activity. Cell *135*, 137–148.

Yoshimura, T., Arimura, N., and Kaibuchi, K. (2006). Signaling networks in neuronal polarization. J. Neurosci. *26*, 10626–10630.

Zaoui, K., Benseddik, K., Daou, P., Salaün, D., and Badache, A. (2010). ErbB2 receptor controls microtubule capture by recruiting ACF7 to the plasma membrane of migrating cells. Proc. Natl. Acad. Sci. USA *107*, 18517–18522.